NIH Public Access
Author Manuscript
Cell. Author manuscript; available in PMC 2013 April 03.

Published in final edited form as:
Cell. 2012 February 3; 148(3): 543–555. doi:10.1016/j.cell.2012.01.016.

PKCε regulates ATF2 availability to alter mitochondrial permeability following genotoxic stress

Eric Lau[1], **Harriet Kluger**[2], **Tal Varsano**[1], **KiYoung Lee**[3,4], **Immo Scheffler**[5], **David L. Rimm**[2], **Trey Ideker**[2], and **Ze'ev A. Ronai**[1]

[1]Signal Transduction Program, Sanford-Burnham Medical Research Institute, La Jolla, CA, 92037, USA

[2]Department of Medicine, Yale University, New Haven, CT 06520, USA

[3]Departments of Medicine and Bioengineering University of California San Diego, La Jolla, CA 92093 USA

[4]Department of Biomedical Informatics, Ajou University School of Medicine, Suwon 443-749, Korea

[5]Department of Biology, University of California San Diego, La Jolla, CA, 92093 USA

Summary

The transcription factor ATF2 elicits oncogenic activities in melanoma and tumor suppressor activities in non-malignant skin cancer. Here we identify that ATF2 tumor suppressor function is determined by its ability to localize at the mitochondria, where it alters membrane permeability following genotoxic stress. The ability of ATF2 to reach the mitochondria is determined by PKCε, which directs ATF2 nuclear localization. Genotoxic stress attenuates PKCε effect on ATF2, enables ATF2 nuclear export and localization at the mitochondria, where it perturbs the HK1-VDAC1 complex, increases mitochondrial permeability and promotes apoptosis. Significantly, high levels of PKCε, as seen in melanoma cells, block ATF2 nuclear export and function at the mitochondria, thereby attenuating apoptosis following exposure to genotoxic stress. In melanoma tumor samples, high PKCε levels associates with poor prognosis. Overall, our findings provide the framework for understanding how subcellular localization enables ATF2 oncogenic or tumor suppressor functions.

Introduction

Activating Transcription Factor 2 (ATF2) is one of sixteen Atf/Creb family transcription factors and an integral component of the Activator Protein-1 (AP-1) transcriptional complex, which regulates normal cellular growth and development, as well as cellular response to stress (Lopez-Bergami et al., 2010). The diverse transcriptional functions of ATF2 are attributed to its homo- or heterodimerization with other AP-1 transcription factors via a basic leucine zipper (bZIP) domain, in concert with its phosphorylation by stress kinases, JNK or p38, on residues 69/71 (Gupta et al., 1995). As a stress-inducible transcription

© 2012 Elsevier Inc. All rights reserved.

Correspondence: Ze'ev A. Ronai, Signal Transduction Program, Sanford-Burnham Medical Research Institute, 10901 N. Torrey Pines Rd, La Jolla, CA, 92037 USA, ronai@sbmri.org.

Publisher's Disclaimer: This is a PDF file of an unedited manuscript that has been accepted for publication. As a service to our customers we are providing this early version of the manuscript. The manuscript will undergo copyediting, typesetting, and review of the resulting proof before it is published in its final citable form. Please note that during the production process errors may be discovered which could affect the content, and all legal disclaimers that apply to the journal pertain.

NIH-PA Author Manuscript
NIH-PA Author Manuscript
NIH-PA Author Manuscript

NIH-PA Author Manuscript

NIH-PA Author Manuscript

NIH-PA Author Manuscript

factor, ATF2 regulates gene expression programs implicated in cell cycle control, cytokine expression and cell death (Lopez-Bergami et al., 2010). In addition to its transcriptional role, ATF2 functions in the DNA damage response, which requires ATM-dependent phosphorylation on residues 490/498. Mice harboring mutations at these sites are more radiosensitive and genetically unstable when crossed with p53 mutant mice or when subjected to a skin carcinogenesis protocol (Bhoumik et al., 2005; Li et al., 2010).

While the above functions require nuclear localization, growing evidence points to cytoplasmic localization of ATF2, although its function there remains elusive. In melanomas, nuclear ATF2 is associated with metastasis and poor prognosis, whereas cytoplasmic ATF2 is associated with non-malignant skin cancers and better prognosis (Berger et al., 2003). ATF2 transcriptional activity (which requires nuclear localization) is required for melanoma development, as demonstrated in the N-Ras/Ink4a mouse melanoma model (Shah et al., 2010). Correspondingly, inhibition of ATF2 nuclear localization by expression of either 10 or 50 amino acid (aa) peptides derived from ATF2 efficiently attenuates melanoma development (Bhoumik et al., 2004). In contrast, ATF2 cytosolic localization, as seen in non-malignant skin cancer, is associated with a tumor suppressor role; inhibiting ATF2 in keratinocytes results in a greater number of skin papillomas that develop more rapidly than do control cells (Bhoumik et al., 2008).

We investigated mechanisms underlying the ability of ATF2 to elicit diverse nuclear and cytoplasmic functions and report that ATF2 functions at the mitochondria in response to genotoxic stress. We found that at the mitochondrial outer membrane, ATF2 abrogates formation of high order complexes containing hexokinase-1 (HK1) and voltage-dependent anion-channel-1 (VDAC1), deregulating mitochondrial outer membrane permeability and initiating apoptosis. This function is negatively regulated by PKCε phosphorylation of ATF2, which dictates its nuclear localization. Notably, elevated expression and activity of PKCε was reported in different tumor types, and is associated with poorer outcome and inhibition of tumor cell death (Bae et al., 2007). Whereas PKCε overexpression promotes the development of squamous carcinomas (Sand et al., 2010), its inhibition sensitizes tumor cells to cell death (Gillespie et al., 2005). The identification of mechanisms underlying ATF2 subcellular localization and cytosolic function offer a framework for understanding the regulation of opposing functions for the same transcription factor.

Results

Genotoxic stress induces ATF2 nuclear export and mitochondrial localization

Although ATF2 cytoplasmic localization was previously reported (Berger et al., 2003; Bhoumik et al., 2008; Deng et al., 2008), a cytoplasmic function has yet to be described. Based on the observed cytosolic localization of ATF2 in squamous cell carcinoma (SCC) tumors, we employed an SCC line (SCC9) to analyze potential ATF2 cytoplasmic function. Mass spectrometric (MS) analysis of cytosol-localized ATF2-bound proteins in SCC9 cells identified a cluster of mitochondria-outer membrane related proteins, suggesting an ATF2 mitochondrial interaction (Table S1). Indeed, non-stressed SCC9 cells exhibit predominantly nuclear ATF2, whereas genotoxic stress rendered by etoposide (ETO) resulted in its accumulation at mitochondria in ~64% of treated cells (Figure 1A). Other genotoxic insults, including ultraviolet C (UVC, 20 J/m^2) and ionizing irradiation (IR, 5Gy) also prompted the mitochondrial localization of ATF2 (Figure 1A). The mitochondrial localization of ATF2 following genotoxic stimuli was also seen in other cell types, including normal human fibroblasts (HSF), primary human keratinocytes (NHEK) and melanocytes (HEM), as well as in other SCC cell lines (M7 and P9)(Figure S1). Notably, whereas some melanoma cell lines (UACC903) exhibit partial mitochondrial enrichment of ATF2 (Figure S1 & 6D), a number of melanoma cell lines (LU1205 and 501Mel, Figure S1 & 6D) did not exhibit

NIH-PA Author Manuscript

NIH-PA Author Manuscript

NIH-PA Author Manuscript

mitochondrial localization of ATF2 following genotoxic stimuli, with the exception of IR (Figure S1), suggesting that malignant melanomas are largely resistant to genotoxic stress-induced mitochondrial translocation of ATF2. The extent of ATF2 mitochondrial localization differs among the different cultures and type of stimuli, indicating variation in cellular response and control of such translocation in each of these cultures. Biochemical fractionation of SCC9 cells confirmed that exposure to genotoxic stress results in the accumulation of ATF2 in mitochondrial-enriched fractions (Figure 1B).

Pre-treatment of SCC9 cells with the nuclear export inhibitor, leptomycin B (LMB), prevented mitochondrial accumulation of ATF2 following ETO treatment, indicating that nuclear export of ATF2 occurs after genotoxic stress (Figure 1A, 5th row). Consistently, we observed a ~50% reduction of luciferase activity driven by the ATF2 response element (Figure 1C).

ATF2 protein does not harbor canonical mitochondrial localization or peptide-processing signals, which could facilitate import or insertion into mitochondrial membranes, suggesting that its mitochondrial localization requires interaction with mitochondrial protein(s). Thus, we examined where ATF2 might be accumulating at the mitochondrial outer membrane (MOM), the intermembrane space (IMS), the mitochondrial inner membrane (MIM), or the mitochondrial inner matrix. Limited proteolysis protection assays with enriched mitochondrial fractions purified from ETO-treated SCC9 cells revealed efficient degradation of ATF2 in the absence of detergent, consistent with the degradation pattern of the MOM component, TOM20, but differing from the pattern of inner matrix protein, COXII, which is degraded only in the presence of detergent (Figure 1D). These results suggest that in response to genotoxic stress, ATF2 localizes at the MOM.

ATF2 interacts with HK1:VDAC1 complexes following genotoxic stress

To determine ATF2 function at mitochondria, we tested MOM protein(s) identified in our MS analysis (Table S1), Hexokinase-1 (HK1), and Voltage-Dependent Anion Channel 1 (VDAC1) (Figure S1), for possible interaction with ATF2.

In response to various forms of stress, HK1 and HK2 bind to VDAC1, which oligomerizes to form large molecular weight complexes (Abu-Hamad et al., 2009). To determine whether ATF2 is part of these complexes, we assessed the distribution of ATF2, HK1 and VDAC1 in fractions obtained following fast protein liquid chromatographic (FPLC) analysis using a gel filtration column. Whereas prior to stress, ATF2 did not co-distribute to fractions with HK1 and VDAC1, after ETO treatment, all three proteins were found within high molecular weight fractions (Figure 2A). Notably, not all of the ATF2 protein re-distributed to high MW fractions. The remaining ATF2 in the low MW fraction is consistent with the residual nuclear ATF2 found by IHC and the residual (~50%) transcriptional activity recorded after ETO treatment (Figures 1A and 1C, respectively). As shown below, distinct post-translational modification of ATF2 are found in these pools.

To confirm the interaction of ATF2 with HK1 and VDAC1, we immunoprecipitated endogenous ATF2 or HK1 from cell lysates of SCC9 cells prior to and after ETO treatment. ATF2 interaction with HK1 and with high molecular weight (~130 kDa) tetrameric VDAC1 oligomers, detectable with the aid of crosslinker (Zalk et al., 2005), was clearly seen after ETO treatment (Figure 2B, upper and lower). Interestingly, knockdown of HK1, but not HK2, abrogated mitochondrial localization of ATF2 following ETO treatment, indicating that the mitochondrial localization of ATF2 requires HK1 (Figure 2C, 2D and S2A).

NIH-PA Author Manuscript

NIH-PA Author Manuscript

NIH-PA Author Manuscript

PKCε-phosphorylation negatively regulates ATF2 mitochondrial localization

Phosphorylation of ATF2 by p38 or JNK on Thr69/71 is required for its dimerization with AP-1 transcription factors and for transcriptional activity (Gupta et al., 1995; van Dam et al., 1995). However, Thr69/71 phosphorylation was dispensable for ATF2 mitochondrial localization, as inhibition of either p38 or JNK activity by respective pharmacological inhibitors did not alter its nuclear localization (Figure S2B).

Analysis of ATF2 protein sequence using the phosphorylation site scanning program (http://scansite.mit.edu) predicted an uncharacterized, but highly probable PKCε/δ/ζ phosphorylation site on residue Thr52. Treatment with the PKCε translocation inhibitor (PKCε-i) promoted mitochondrial localization of ATF2, even in the absence of ETO, as detected by both IHC and mitochondrial fractionation (Figure 3A, S3F). Consistently, siRNA-mediated knockdown of PKCε (Figure S3A) promoted mitochondrial localization of ATF2 (Figure 3B), while overexpression of a constitutively active form of PKCε (caPKCε; Pass et al., 2001), attenuated ATF2 accumulation at mitochondria following ETO treatment (Figure 3C). As with the genotoxic stress-induced nuclear export of ATF2 (Figure 1A), LMB pre-treatment blocked its mitochondrial translocation following PKCε inhibition (Figure S3E). Inhibition of the novel (δ) or atypical (ζ), PKC forms had negligible effect on mitochondrial ATF2 localization (Figure S3B). These observations indicate that ATF2 mitochondrial localization is primarily regulated by PKCε. Notably, Ser729 phosphorylation on PKCε, an indicator of active PKCε, decreases following overnight treatment with ETO or with PKCε-i (Figure 3D), suggesting that the effect of PKCε on the nuclear localization of ATF2 is attenuated following genotoxic stress, enabling ATF2 nuclear export and mitochondrial localization.

To determine whether the predicted ATF2 site (Thr52) for phosphorylation by PKCε regulates mitochondrial translocation of ATF2, we assessed PKCε phosphorylation of ATF2 in vitro, as well as the localization of $ATF2^{T52A}$ (a non-phosphorylatable alanine phosphomutant) and $ATF2^{T52E}$ (a glutamic acid phosphomimic). In vitro kinase assays employing an ATF2 fragment consisting of aa 50–100 revealed that PKCε phosphorylates the wild type (WT) but not the $ATF2^{T52A}$ peptide. Addition of PKC catalytic inhibitor Gö6850 inhibited this phosphorylation (Figure 3E). Together, these data indicate that Thr52 is a PKCε phosphoacceptor site. Consistent with the nuclear localization observed in the presence of caPKCε, the $ATF2^{T52E}$ mutant exhibited constitutive nuclear localization (Figure 3F), whereas the $ATF2^{T52A}$ mutant localized to the cytoplasm and mitochondria, even in the absence of genotoxic stress (Figure 3F). Gel filtration analysis revealed that, $ATF2^{T52A}$, but not $ATF2^{T52E}$, distributed to large molecular weight fractions containing VDAC1 (Figure S3D). Interestingly, expression of $ATF2^{T52A}$ revealed less HK1 within the high molecular weight VDAC1-containing fractions, pointing to the possibility that $ATF2^{T52A}$ may attenuate the interaction between HK1 and VDAC1. Collectively, these findings establish that PKCε regulates ATF2 mitochondrial localization via phosphorylation at T52.

Given the effect of PKCε on ATF2 subcellular localization, we next assessed its effect on ATF2 transcriptional activity. Overexpression of caPKCε led to a marked increase in Jun2-luciferase activity, indicative of ATF2 transcriptional activity, which was largely attenuated upon knockdown of ATF2 (Figure 3G). Interestingly, inhibition with Gö6850 or ETO treatment reduced Jun2-luciferase activity to similar extents as knockdown of ATF2, suggesting that PKCε contributes to basal transcriptional activity of ATF2 in these cells. Consistently, reconstitution of SCC9 cells carrying a stable-knockdown of ATF2 (employing shRNA targeting ATF2 3′-UTR, Figure S3C) with $ATF2^{T52E}$ also increased Jun2-luciferase activity compared to $ATF2^{WT}$. Conversely, mutation of T52 to alanine abolished ATF2 transcriptional activity (Figure 3H). These findings indicate that by

NIH-PA Author Manuscript

NIH-PA Author Manuscript

NIH-PA Author Manuscript

regulating ATF2 nuclear localization, PKCε not only determines ability of ATF2 to reach the mitochondria, but also its transcriptional activity.

Mitochondria-localized ATF2 compromises outer-membrane integrity by disrupting HK1:VDAC1 complexes

Disruption of VDAC interaction with HK1 or HK2 sensitizes cells to stress, promoting MOM leakage of molecules from the IMS (Abu-Hamad et al., 2009). Conversely, HK1 or HK2 binding to the MOM promotes resistance to stress and increased cell survival (Moin et al., 2007; Shoshan-Barmatz et al., 2010; Shulga et al., 2009). To assess whether interaction with ATF2 perturbs the HK1/VDAC1 complex, we first evaluated HK1 accumulation at mitochondria following ectopic expression of the ATF2 phosphomutants that preferentially localize to either the nucleus ($ATF2^{T52E}$) or mitochondria ($ATF2^{T52A}$) (Figure 4, S4D). Under basal conditions, HK1 is localized to the cytoplasm and mitochondria (Figure 4A). Notably, mitochondrial co-localization of HK1 was enhanced after ETO treatment (Figure 4B). In $ATF2^{T52E}$-transfected cells, HK1 accumulation at mitochondria was similar to that seen in control cells prior and after ETO treatment (Figure 4G, H). However, $ATF2^{T52A}$ overexpression abrogated mitochondrial accumulation of HK1 prior to and following genotoxic stress, as indicated by decreased distinct co-localization of HK1 and MitoTracker (Figure 4E, F and insets 4E*, F*). Notably, ETO-treated, ATF^{T52A}-expressing cells exhibited more fragmented mitochondria compared to cells expressing empty vector, $ATF2^{WT}$ or $ATF2^{T52E}$ (Figure insets 4E* and F*, compared to 4A, B, C, G and H). Further, the expression $ATF2^{T52A}$ promoted the appearance of punctated, HK1-positively staining structures that localized near, but not with the MitoTracker-labeled mitochondrial structures (Figure 4E, F and insets E* and F*, and S4E). These results indicate that mitochondrial translocation of ATF2 perturbs HK1/VDAC1 complexes and MOM integrity. $ATF2^{WT}$ also translocated to the mitochondria and abrogated HK1 localization following genotoxic stress, (Figure 4D). Expression of either $ATF2^{WT}$ or the T52 ATF2 mutants did not affect VDAC1 multimerization, a change that promotes mitochondrial leakage and cell death, as assessed by crosslinking and non-reducing immunoblot analysis (data not shown).

Consistent with our IHC data, overexpression of $ATF2^{T52A}$ abrogated HK1 association with VDAC1 that was immunprecipitated under basal conditions and following genotoxic stress. Overexpression of $ATF2^{WT}$ abrogated the HK1/VDAC1 complex only after ETO treatment, whereas the $ATF2^{T52E}$ did not affect HK1 binding to VDAC1 (Figure 5A). In agreement, HK1 association with VDAC1 also decreased following treatment of SCC9 cells with PKCε-i alone or PKCε-i in the presence of ETO (Figure 5B). These data indicate that mitochondria-localized ATF2 attenuates the ability of HK1 to form a complex with VDAC.

ATF2 localization at the mitochondria reduces mitochondrial potential and sensitizes cells to genotoxic stress-induced death

We next monitored changes in mitochondrial membrane potential that are reflective of leakage. We used fluorescence-activated cell sorting (FACS) to quantify tetramethylrhodamine ethyl ester (TMRE) uptake, an indicator of relative mitochondrial membrane potential. Consistent with previous reports (Fu et al., 2008), low-dose ETO initially increased TMRE uptake by control SCC9 cells (Figure S4A), whereas increased doses of ETO reduced TMRE uptake (data not shown).

$ATF2^{T52E}$-transfected SCC9 cells did not exhibit altered TMRE uptake compared to empty vector- (EV) or $ATF2^{WT}$ –transfected cells. These, as well as EV-transfected cells, increased TMRE uptake following genotoxic stress (Figure S4A). In contrast, $ATF2^{T52A}$ –transfected cells decreased TMRE uptake (Figure S4A, S4C), consistent with our IHC data

NIH-PA Author Manuscript

NIH-PA Author Manuscript

NIH-PA Author Manuscript

indicating that mitochondrial ATF2 impairs the formation of HK1/VDAC1 complexes, and thus MOM integrity.

As changes in the absolute number of mitochondria (mitochondrial mass) need to be monitored in order to determine net changes in mitochondrial potential, we pulse-labeled SCC9 cells with nonyl-acridine orange (NaO) to stain for cardiolipin, a mitochondrial lipid that is unaffected by altered membrane potential. $ATF2^{T52A}$- but not $ATF2^{T52E}$-expressing cells, increased NaO staining, indicating that loss of mitochondrial membrane potential increased mitochondrial biogenesis, likely to compensate for dysfunctional mitochondria (Figure S4B, S4C), consistent with previous reports (Fu et al., 2008). Notably, the observed TMRE/NaO ratios, reflective of membrane potential per mitochondria (mitochondrial "leakiness"), indicate that overexpression of $ATF2^{T52A}$, but not of $ATF2^{WT}$ or $ATF2^{T52E}$, decreases membrane potential relative to control cells (Figures 5C). Correspondingly, only $ATF2^{T52A}$ expression induced cytochrome C leakage (Figure 5C, S5D). Interestingly, the IHC pattern of cytochrome C release is reflective of partial leakage (Carvalho et al., 2004), suggesting that mitochondrial ATF2 serves as a priming/initial trigger for sensitization, which precedes cell death. That $ATF2^{WT}$ expression did not decrease mitochondrial potential or induce cell death (Figure 5D) could be explained by its susceptibility to be phosphorylated on T52 and retained in the nucleus. Hence, partial inhibition of PKCε is expected to allow partial nuclear retention of ATF2, whereas $ATF2^{T52A}$ is largely excluded from the nuclei. Indeed, nuclear localization is seen in ~40% of the $ATF2^{WT}$-expressing cells (Figure S4D), which may dampen the effect elicited by the cytosolic ATF2. These observations suggest that a minimal level of ATF2 must reach the mitochondria in order to affect membrane potential and to promote cell death.

As mitochondrial leakage often precedes cell death, we evaluated whether mitochondria-localized ATF2 would sensitize cells to genotoxic stress-induced cell death. We examined how PKCε inhibition affected SCC9 cells exposed to genotoxic stress. Cells treated with PKCε-i exhibited increased Annexin-V labeling, similar to ETO-treated cells (Figure 5E). The latter is consistent with the observation that PKCε activation was equally attenuated upon ETO or PKCε-i treatment (Figure 3D). Furthermore, cells subjected to PKCε-i or siRNA-mediated knockdown of PKCε also exhibited increased cell death after ETO or UVC (20 J/m^2) treatment (Figure S5A, S5B). Consistently, expression of $ATF2^{T52A}$ but not $ATF2^{WT}$ or $ATF2^{T52E}$ also resulted in elevated cell death, regardless of genotoxic stress (Figure 5F).

Given the importance of Bax in the permeabilization of mitochondria and control of cell death, we assessed possible changes in the conformation, and thus activation, of Bax. Using antibodies recognizing active conformation of BAX, we revealed that $ATF2^{T52A}$ promotes active Bax conformation, whereas $ATF2^{T52E}$ attenuates such conformation (Figure S5E).

PKCε expression increases T52 phosphorylation of ATF2 and melanoma cells resistance to genotoxic stress

To monitor PKCε phosphorylation of ATF2 on T52, we generated a polyclonal antibody against phosphorylated T52 (pT52 antibody). caPKCε overexpression in SCC9 cells resulted in the appearance of a slower migrating band that was recognized by total and pT52 ATF2 antibodies (Figure 6A). Both total ATF2 and pT52 ATF2 bands were no longer detectable upon ATF2 knockdown (Figure 6B).

We next evaluated the status of pT52 in SCC9 as well as melanoma cell lines prior to and after genotoxic stress. Consistent with reduced PKCε phosphorylation of ATF2 on T52, pT52 levels were lower in SCC9 cells subjected to ETO treatment (Figure 6C). Notably, whereas decreased T52 phosphorylation was also apparent in ETO-treated UACC903 cells,

NIH-PA Author Manuscript

NIH-PA Author Manuscript

NIH-PA Author Manuscript

it was much less pronounced in 501Mel and LU1205 cells. These findings are consistent with the relationship between PKCε activity and the ability of ATF2 to translocate to the mitochondria following genotoxic stress. Respectively, UACC903, but not LU1205 or 501Mel cells, exhibited partial mitochondrial translocation of ATF2 following ETO treatment (Figure 6C and D). Correspondingly, LU1205 and 501Mel cells were more resistant to cell death compared with UACC903, SCC9 or P9 (an SCC line with low PKCε levels, Figure S6A), further supporting the notion that melanoma resistance to genotoxic stress-induced cell death is due to impaired mitochondrial translocation of ATF2. Consistent with these observations and the nuclear localization of the $ATF2^{T52E}$ mutant, immunostaining with the pT52 antibody detected only nuclear ATF2 (Figure S7A). These findings suggest that elevated PKCε levels in melanoma cells inhibit ATF2 localization and function at the mitochondria, thereby attenuating its role in promoting cell death following genotoxic stress.

To establish the relationship between PKCε activity, pT52 phosphorylation and sensitization to genotoxic stress-induced apoptosis, we manipulated PKCε or ATF2 in MEL501 and SCC9 cells. Whereas MEL501 cells exhibit high levels of PKCε, T52 phosphorylation and impaired ATF2 translocation to the mitochondria (Figure 6C, 6D and 7A), SCC9 have low levels of PKCε, T52 phosphorylation and exhibit ATF2 localization at the mitochondria following genotoxic stress (Figure 1, 6C and 7A). ETO or UVC treatment, combined with PKCε-i or expression of PKCε-targeted siRNA, sensitized 501MEL to genotoxic stress-induced cell death (Figure 6E; S5C). Conversely, $ATF2^{T52E}$-expressing SCC9 cells exhibited lower levels of the early apoptotic marker Annexin-V in response to ETO, PKCε-i, or a combination of both, compared to EV- or $ATF2^{WT}$ –expressing cells (Figure S6B), corroborating the pro-survival function associated with T52 phosphorylation. Intriguingly, although stable EV, $ATF2^{WT}$ or $ATF2^{T52E}$ expression in SCC9 cells produced no significant effects in proliferation rate during non-stressed conditions, $ATF2^{T52E}$ conferred a survival advantage when the cells were grown in the presence of ETO (Figure S6C), further demonstrating the pro-survival effects conferred by pT52-ATF2.

High expression of PKCε in melanoma tumors is associated with poor prognosis

To assess the nature of the differences in genotoxic stress resistance between melanoma and SCC cells, we surveyed the degree of PKCε expression and activity in a panel of melanoma cell lines and a large cohort melanoma tissue arrays (TMA). Overall, melanoma cell lines exhibited higher PKCε expression than primary keratinocytes, melanocytes, or SCC lines (Figure 7A). Notably, pT52 was lowest in primary keratinocytes and melanocytes, whereas its levels were highest in 501Mel and LU1205, where total and pS729 (active) PKCε levels are the highest.

We next studied the association between PKCε expression levels, patient survival, and other clinical and pathological factors. IHC of a melanoma TMA revealed fairly homogenous cytoplasmic/membranous staining within each histospot (Figure S7B). Immunofluorescent intensity was measurable in 427 histospots (171 primary and 256 metastatic cases).

PKCε expression was higher in metastastic than primary specimens ($P < 0.0001$), as shown in Figure 7B. In primary specimens, PKCε levels were higher in thicker lesions ($P < 0.0001$) and in ulcerated lesions ($P = 0.0004$). PKCε expression did not correlate with age, gender or presence of tumor infiltrating lymphocytes.

Cox univariate survival analysis of continuous immunofluorescent intensity scores indicated that high PKCε expression was associated with decreased survival in the primary cohort ($P = 0.0042$), but not in the metastatic subset ($P = 0.887$). Multivariate analysis of PKCε expression did not retain its independent prognostic value, presumably due to the strong

NIH-PA Author Manuscript

NIH-PA Author Manuscript

NIH-PA Author Manuscript

association with Breslow Depth. To visually demonstrate the association between PKCε expression and survival, we dichotomized the continuous scores by the median score. High PKCε expression was not associated with survival in the metastatic subset of patients (log rank $P = 0.8$; Figure S7C), but rather, was strongly associated with decreased survival in the primary cohort (log rank $P = 0.0004$; Figure 7C), consistent with our earlier analyses of a similar cohort in which nuclear localization of ATF2 correlated with poor prognosis (Berger et al., 2003).

Recent global mRNA expression profiling analyses (Yu et al., 2008) revealed that ATF2 and VDAC1 expression are highly correlated in non-malignant tissue samples, but significantly less correlated in basal cell carcinoma (Figures S7D, E). Independent expression profiling of metastatic versus non-metastatic melanoma (Xu et al., 2008) also identified that ATF2 and VDAC1 expression are significantly more correlated in primary melanoma than in aggressive metastases (Figure S7F, G). These analyses are consistent with ability to predict cancer outcome using dynamic modularity in protein interaction networks (Taylor et al., 2009).

Discussion

A number of transcription factors including, Myc, Notch, and β-catenin, exhibit both oncogenic and tumor suppressor activities (Koch and Radtke, 2007; Larsson and Henriksson, 2010), yet, the mechanism(s) controlling their opposing functions are largely associated with a given tissue/cell type. Here, we demonstrate that the tumor suppressor or oncogenic activities of ATF2 result from its cytosolic or nuclear function, respectively (Figure 7E). Cytosolic localization of ATF2 has been seen in non-malignant skin tumors where ATF2 exhibits tumor suppressor activity. Thus, mice expressing a transcriptionally inactive form of ATF2 in keratinocytes developed more rapid and larger skin papillomas than wild type mice, when subjected to DMBA-TPA skin carcinogenesis (Bhoumik et al., 2008). In addition, p53 mutant mice lacking ATF2 in mammary tissues had a higher incidence of mammary tumors (Maekawa et al., 2008). In contrast to these tumor suppressor activities, ATF2 plays an oncogenic role in malignant melanoma. Inactivation of ATF2 in melanocytes attenuates melanoma formation in the mutant N-Ras/Ink4a model (Shah et al., 2010). Unlike in BCC/SCC where ATF2 is also cytosolic, ATF2 is predominantly nuclear in melanoma, which is associated with poor prognosis (Berger et al., 2003).

The present findings reveal that following genotoxic stress, cytosolic ATF2 impairs HK1/VDAC1 complexes and mitochondrial membrane integrity, sensitizing cells to apoptosis. In contrast, the high PKCε expression in melanoma cells induces predominantly nuclear localization of ATF2, which attenuates its normal cytosolic function and correlates with resistance to genotoxic stress. Notably, the different levels of PKCε activity found in melanomas determine the extent to which ATF2 reaches the mitochondria and promotes cell death following genotoxic stress. Thus, PKCε dictates the tumor suppressor or oncogenic activities of ATF2 by directly affecting its nuclear or cytosolic localization.

While transcription factors such as p53, CREB, Stat3, and Elk-1 have been reported to localize at the mitochondria (Barrett et al., 2006; Lee et al., 2005; Mihara et al., 2003; Wegrzyn et al., 2009), the finding that ATF2 can switch between its oncogenic transcriptional function and its tumor suppressor mitochondrial function presents a new paradigm for transcription factor regulation and function. We show that the ability of ATF2 to abrogate the HK1/VDAC complex is perturbed in melanomas, which offers insight into the mechanisms underlying the notorious resistance of melanoma to therapy. Consistent with this, HK/VDAC1 complexes are increased in cancer cells and are associated with induction of the Warburg effect and a tumorigenic advantage (Mathupala et al., 2006).

NIH-PA Author Manuscript

NIH-PA Author Manuscript

NIH-PA Author Manuscript

PKCε may play an indirect role in the metabolic changes that contribute to cancer development and/or progression, as suggested by the observation that elevated PKCε activity antagonizes the HK1/VDAC1-perturbing function of ATF2. Notably, Bax activation is induced by $ATF2^{T52A}$ and reduced by $ATF2^{T52E}$ (Figure S5E), which may be associated with the effect seen on HK1/VDAC or reflective of additional activities elicited by cytosolic/mitochondrial ATF2.

Multivariate analysis did not identify PKCε expression as an independent prognostic marker for melanoma, implying that it may not be a driver of melanoma progression. This would be consistent with our finding that $ATF2^{T52E}$ confers a survival advantage during genotoxic stress, but does not confer a proliferative advantage (Figure S6B, C) or anchorage-independent growth (data not shown). The upregulation of PKCε seen in metastatic melanomas explains how ATF2 mitochondrial function is attenuated and why nuclear localization of ATF2 is associated with poor prognosis in melanoma. Although many cancers show a correlation between elevated PKCε expression/activity and poor prognosis and chemotherapeutic resistance, the ATF2 status in these tumors is unknown (Bae et al., 2007). Notably, efforts to target PKCε for cancer therapy have met with limited success, primarily because of its similarity to PKCδ (Gonelli et al., 2009). Small molecules that induce cytosolic localization of ATF2 may thus represent a new class of compounds with a unique advantage for therapy, and more specific PKCε inhibitors may also be effective in this capacity.

We previously identified 10- and 50-aa ATF2-derived peptides that inhibited the transcriptional activity and increased the cytosolic localization of ATF2 (Bhoumik et al., 2004). These peptides (which encompassed T52) sensitized melanoma cells to apoptosis and inhibited melanoma growth in syngeneic mice and in human melanoma xenografts (Bhoumik et al., 2002). Based on our current findings, we propose that these peptides competitively inhibited PKCε phosphorylation of endogenous ATF2, thereby enabling its cytosolic localization and mitochondrial function. Consistent with this, mutation of T52 within the peptides abolished their inhibitory effects (Bhoumik et al., 2004). Strikingly, the amino acid sequences flanking T52 showed marked similarities to known PKC peptide inhibitors, and satisfied the requirements for optimal PKC substrate sequence (Nishikawa et al., 1997). While most PKC isoenzymes strongly prefer peptides with basic amino acids at the −2 position, PKCε also accepts glutamic acid, which is the residue found at this position in the ATF2 peptide (Fig 7D).

Our findings suggest a need to re-evaluate the functional significance of T52 phosphorylation by PKCε to ATF2 transcriptional activity, and the relationship to phosphorylation on Thr69/71 by JNK/p38. We showed that caPKCε induces ~25-fold increase in Jun2-promoter activity, compared to only ~6-fold increased activity induced by $ATF2^{T52E}$ (Figure 3G, H), suggesting that PKCε may augment ATF2 phosphorylation by JNK, p38, or other PKC isoforms (Yamasaki et al., 2009). T52 phosphorylation of ATF2 may also affect the transcriptional function of ATF2 or its heterodimerization partners (Liu et al., 2006), and/or the role of ATF2 in the DNA damage response, which requires its phosphorylation on S490/498 by ATM (Bhoumik et al., 2005).

Collectively, our results establish the role of ATF2 at the mitochondria following genotoxic stress, and reveal its contribution to stress-induced cell death. The degree of PKCε phosphorylation of ATF2 is instrumental in controlling its function. PKCε phosphorylation determines the ability of ATF2 to function at the mitochondria, where its contribution to cell death is consistent with its tumor suppressor functions. Constitutively high PKCε expression/activity, as seen in melanomas, attenuates ATF2 mitochondrial function and enhances its nuclear transcriptional activity, consistent with its oncogenic activity. Thus,

NIH-PA Author Manuscript

NIH-PA Author Manuscript

NIH-PA Author Manuscript

PKCε regulates the subcellular localization of ATF2, which dictates its ability to elicit oncogenic or tumor suppressor activities.

Experimental Procedures

Cell Lines

Squamous cell carcinoma (SCC9) cells were maintained in Dulbecco's Modified Eagle's Medium (DMEM):F-12 (50:50) (Hyclone/Thermo Scientific, USA) supplemented with 400 ng/ml hydrocortisone, 10% fetal bovine serum (FBS) and antibiotics. Melanoma cell lines, M7, P9 and human skin fibroblasts were maintained in Dulbecco's Modified Eagle's Medium (DMEM) supplemented with 10% FBS and antibiotics. Normal human embryo kidney (NHEK) cells were maintained in KGM-2 growth medium (Lonza, USA). Melanocytes were maintained in 254 Medium (Invitrogen, CA, USA).

Antibodies and immunostaining reagents

Antibodies employed were purchased as follows: ATF2 (20F1), HK1 (C35C4), HK2 (C64G5), HA (C29F4—for immunoblot analysis), COXIV (3E11) from Cell Signaling Technologies (MA, USA); β-actin (9), HIS-probe (H-15), HSP90 (4F10), Lamin A (N-16), PKCε (C15), TOM20 (F-10), VDAC1 (20B12) from Santa Cruz Biotechnology, Inc. (CA, USA); HA (3F10—for immunofluorescent staining) from Roche; COXI (21C11BC11), COXII (2E3), COX IV (20E8), pS729 PKCε (44977G) from Invitrogen (CA, USA); HSP60 (24) from BD Pharmingen, USA; pT52 ATF2 (PhosphoSolutions, CO, USA); and Bax (6A7) from ExAlpha Biologicals (MA, USA). MitoTracker Red CMXRos, PKCε translocation inhibitor, Gö6850, and Leptomycin B were purchased from Invitrogen (CA, USA), Santa Cruz Biotechnologies, (CA, USA), EMD Chemicals (NJ, USA), and Sigma (USA), respectively.

Immunocytochemical analysis

After indicated treatments, coverslip-grown cells were fixed in fixation buffer for 20 min at room temperature. Coverslips were then rinsed twice in phosphate buffer solution and permeabilized in permeabilization buffer for 20 min. Primary antibodies were applied at 1:250 dilution in staining buffer overnight at 4°C in a humid chamber. Coverslips were subsequently subject to 5 standing 5-minute washes in wash buffer. Secondary antibodies (Alexa Fluor secondary 350, 488 or 568, Invitrogen) were applied at 1:250 dilution in staining buffer for 2–3 h at room temperature in a humid chamber in the dark. Prior to mounting with Vectorshield with DAPI (Vector Laboratories, CA), coverslips were washed twice more in wash buffer. Immunofluorescent analysis was conducted on an Olympus TH4-100 fluorescent microscope. ≥ 3 Z-planes per field were captured and analyzed using Slidebook V.4.1, and Z-projection images of average intensity were constructed using ImageJ V.1.43u.

Additional Experimental Procedures are online at XXXX

Supplementary Material

Refer to Web version on PubMed Central for supplementary material.

Acknowledgments

We thank Meenhard Herlyn and John Clifford for melanoma and SCC cell lines, Jorge Moscat and Maria Diaz-Meco for PKC reagents, members of the Salvesen lab, Robbin Newlin and Yoav Altman for technical assistance, and Colin Goding for helpful comments on the manuscript. We also thank Ronai laboratory members, Meifan Chen, Hyungsoo Kim, Ersheng Kuang, Marzia Scortegagna and Meera Shah for technical advice and assistance,

NIH-PA Author Manuscript

NIH-PA Author Manuscript

NIH-PA Author Manuscript

and Gustavo Gutierrez for bacterial ATF2 proteins. Support from ACS Postdoctoral Fellowship, Illinois Division and NCI T32 training grant (117090-PF-09-112-01-GMC and 5-T32-CA121949 to EL) and NCI grants (CA099961 and CA051995 to ZR) are gratefully acknowledged.

References

Abu-Hamad S, Arbel N, Calo D, Arzoine L, Israelson A, Keinan N, Ben-Romano R, Friedman O, Shoshan-Barmatz V. The VDAC1 N-terminus is essential both for apoptosis and the protective effect of anti-apoptotic proteins. J Cell Sci. 2009; 122:1906–1916. [PubMed: 19461077]

Bae KM, Wang H, Jiang G, Chen MG, Lu L, Xiao L. Protein kinase C epsilon is overexpressed in primary human non-small cell lung cancers and functionally required for proliferation of non-small cell lung cancer cells in a p21/Cip1-dependent manner. Cancer Res. 2007; 67:6053–6063. [PubMed: 17616661]

Barrett LE, Van Bockstaele EJ, Sul JY, Takano H, Haydon PG, Eberwine JH. Elk-1 associates with the mitochondrial permeability transition pore complex in neurons. Proc Natl Acad Sci U S A. 2006; 103:5155–5160. [PubMed: 16549787]

Berger AJ, Kluger HM, Li N, Kielhorn E, Halaban R, Ronai Z, Rimm DL. Subcellular localization of activating transcription factor 2 in melanoma specimens predicts patient survival. Cancer Res. 2003; 63:8103–8107. [PubMed: 14678960]

Bhoumik A, Fichtman B, Derossi C, Breitwieser W, Kluger HM, Davis S, Subtil A, Meltzer P, Krajewski S, Jones N, et al. Suppressor role of activating transcription factor 2 (ATF2) in skin cancer. Proc Natl Acad Sci U S A. 2008; 105:1674–1679. [PubMed: 18227516]

Bhoumik A, Huang TG, Ivanov V, Gangi L, Qiao RF, Woo SL, Chen SH, Ronai Z. An ATF2-derived peptide sensitizes melanomas to apoptosis and inhibits their growth and metastasis. J Clin Invest. 2002; 110:643–650. [PubMed: 12208865]

Bhoumik A, Jones N, Ronai Z. Transcriptional switch by activating transcription factor 2-derived peptide sensitizes melanoma cells to apoptosis and inhibits their tumorigenicity. Proc Natl Acad Sci U S A. 2004; 101:4222–4227. [PubMed: 15010535]

Bhoumik A, Takahashi S, Breitweiser W, Shiloh Y, Jones N, Ronai Z. ATM-dependent phosphorylation of ATF2 is required for the DNA damage response. Mol Cell. 2005; 18:577–587. [PubMed: 15916964]

Carvalho AC, Sharpe J, Rosenstock TR, Teles AF, Youle RJ, Smaili SS. Bax affects intracellular Ca2+ stores and induces Ca2+ wave propagation. Cell Death Differ. 2004; 11:1265–1276. [PubMed: 15499375]

Deng X, Liu H, Huang J, Cheng L, Keller ET, Parsons SJ, Hu CD. Ionizing radiation induces prostate cancer neuroendocrine differentiation through interplay of CREB and ATF2: implications for disease progression. Cancer Res. 2008; 68:9663–9670. [PubMed: 19047143]

Fu X, Wan S, Lyu YL, Liu LF, Qi H. Etoposide induces ATM-dependent mitochondrial biogenesis through AMPK activation. PLoS One. 2008; 3:e2009. [PubMed: 18431490]

Gillespie S, Zhang XD, Hersey P. Variable expression of protein kinase C epsilon in human melanoma cells regulates sensitivity to TRAIL-induced apoptosis. Mol Cancer Ther. 2005; 4:668–676. [PubMed: 15827341]

Gonelli A, Mischiati C, Guerrini R, Voltan R, Salvadori S, Zauli G. Perspectives of protein kinase C (PKC) inhibitors as anti-cancer agents. Mini Rev Med Chem. 2009; 9:498–509. [PubMed: 19356127]

Gupta S, Campbell D, Derijard B, Davis RJ. Transcription factor ATF2 regulation by the JNK signal transduction pathway. Science. 1995; 267:389–393. [PubMed: 7824938]

Koch U, Radtke F. Notch and cancer: a double-edged sword. Cell Mol Life Sci. 2007; 64:2746–2762. [PubMed: 17687513]

Larsson LG, Henriksson MA. The Yin and Yang functions of the Myc oncoprotein in cancer development and as targets for therapy. Exp Cell Res. 2010; 316:1429–1437. [PubMed: 20382143]

Lee J, Kim CH, Simon DK, Aminova LR, Andreyev AY, Kushnareva YE, Murphy AN, Lonze BE, Kim KS, Ginty DD, et al. Mitochondrial cyclic AMP response element-binding protein (CREB)

NIH-PA Author Manuscript NIH-PA Author Manuscript NIH-PA Author Manuscript

mediates mitochondrial gene expression and neuronal survival. J Biol Chem. 2005; 280:40398–40401. [PubMed: 16207717]

Li S, Ezhevsky S, Dewing A, Cato MH, Scortegagna M, Bhoumik A, Breitwieser W, Braddock D, Eroshkin A, Qi J, et al. Radiation Sensitivity and Tumor Susceptibility in ATM Phospho-Mutant ATF2 Mice. Genes Cancer. 2010; 1:316–330. [PubMed: 20740050]

Liu H, Deng X, Shyu YJ, Li JJ, Taparowsky EJ, Hu CD. Mutual regulation of c-Jun and ATF2 by transcriptional activation and subcellular localization. EMBO J. 2006; 25:1058–1069. [PubMed: 16511568]

Lopez-Bergami P, Lau E, Ronai Z. Emerging roles of ATF2 and the dynamic AP1 network in cancer. Nat Rev Cancer. 2010; 10:65–76. [PubMed: 20029425]

Maekawa T, Sano Y, Shinagawa T, Rahman Z, Sakuma T, Nomura S, Licht JD, Ishii S. ATF-2 controls transcription of Maspin and GADD45 alpha genes independently from p53 to suppress mammary tumors. Oncogene. 2008; 27:1045–1054. [PubMed: 17700520]

Mathupala SP, Ko YH, Pedersen PL. Hexokinase II: cancer's double-edged sword acting as both facilitator and gatekeeper of malignancy when bound to mitochondria. Oncogene. 2006; 25:4777–4786. [PubMed: 16892090]

Mihara M, Erster S, Zaika A, Petrenko O, Chittenden T, Pancoska P, Moll UM. p53 has a direct apoptogenic role at the mitochondria. Mol Cell. 2003; 11:577–590. [PubMed: 12667443]

Moin SM, Panteva M, Jameel S. The hepatitis E virus Orf3 protein protects cells from mitochondrial depolarization and death. J Biol Chem. 2007; 282:21124–21133. [PubMed: 17488721]

Nishikawa K, Toker A, Johannes FJ, Songyang Z, Cantley LC. Determination of the specific substrate sequence motifs of protein kinase C isozymes. J Biol Chem. 1997; 272:952–960. [PubMed: 8995387]

Pass JM, Zheng Y, Wead WB, Zhang J, Li RC, Bolli R, Ping P. PKCepsilon activation induces dichotomous cardiac phenotypes and modulates PKCepsilon-RACK interactions and RACK expression. Am J Physiol Heart Circ Physiol. 2001; 280:H946–955. [PubMed: 11179034]

Sand JM, Aziz MH, Dreckschmidt NE, Havighurst TC, Kim K, Oberley TD, Verma AK. PKCepsilon overexpression, irrespective of genetic background, sensitizes skin to UVR-induced development of squamous-cell carcinomas. J Invest Dermatol. 2010; 130:270–277. [PubMed: 19626035]

Shah M, Bhoumik A, Goel V, Dewing A, Breitwieser W, Kluger H, Krajewski S, Krajewska M, Dehart J, Lau E, et al. A role for ATF2 in regulating MITF and melanoma development. PLoS Genet. 2010; 6:e1001258. [PubMed: 21203491]

Shoshan-Barmatz V, Keinan N, Abu-Hamad S, Tyomkin D, Aram L. Apoptosis is regulated by the VDAC1 N-terminal region and by VDAC oligomerization: release of cytochrome c, AIF and Smac/Diablo. Biochim Biophys Acta. 2010; 1797:1281–1291. [PubMed: 20214874]

Shulga N, Wilson-Smith R, Pastorino JG. Hexokinase II detachment from the mitochondria potentiates cisplatin induced cytotoxicity through a caspase-2 dependent mechanism. Cell Cycle. 2009; 8:3355–3364. [PubMed: 19770592]

Taylor IW, Linding R, Warde-Farley D, Liu Y, Pesquita C, Faria D, Bull S, Pawson T, Morris Q, Wrana JL. Dynamic modularity in protein interaction networks predicts breast cancer outcome. Nat Biotechnol. 2009; 27:199–204. [PubMed: 19182785]

van Dam H, Wilhelm D, Herr I, Steffen A, Herrlich P, Angel P. ATF-2 is preferentially activated by stress-activated protein kinases to mediate c-jun induction in response to genotoxic agents. EMBO J. 1995; 14:1798–1811. [PubMed: 7737130]

Wegrzyn J, Potla R, Chwae YJ, Sepuri NB, Zhang Q, Koeck T, Derecka M, Szczepanek K, Szelag M, Gornicka A, et al. Function of mitochondrial Stat3 in cellular respiration. Science. 2009; 323:793–797. [PubMed: 19131594]

Xu L, Shen SS, Hoshida Y, Subramanian A, Ross K, Brunet JP, Wagner SN, Ramaswamy S, Mesirov JP, Hynes RO. Gene expression changes in an animal melanoma model correlate with aggressiveness of human melanoma metastases. Mol Cancer Res. 2008; 6:760–769. [PubMed: 18505921]

Yamasaki T, Takahashi A, Pan J, Yamaguchi N, Yokoyama KK. Phosphorylation of Activation Transcription Factor-2 at Serine 121 by Protein Kinase C Controls c-Jun-mediated Activation of Transcription. J Biol Chem. 2009; 284:8567–8581. [PubMed: 19176525]

NIH-PA Author Manuscript

NIH-PA Author Manuscript

NIH-PA Author Manuscript

Yu M, Zloty D, Cowan B, Shapiro J, Haegert A, Bell RH, Warshawski L, Carr N, McElwee KJ. Superficial, nodular, and morpheiform basal-cell carcinomas exhibit distinct gene expression profiles. J Invest Dermatol. 2008; 128:1797–1805. [PubMed: 18200053]

Zalk R, Israelson A, Garty ES, Azoulay-Zohar H, Shoshan-Barmatz V. Oligomeric states of the voltage-dependent anion channel and cytochrome c release from mitochondria. Biochem J. 2005; 386:73–83. [PubMed: 15456403]

NIH-PA Author Manuscript

NIH-PA Author Manuscript

NIH-PA Author Manuscript

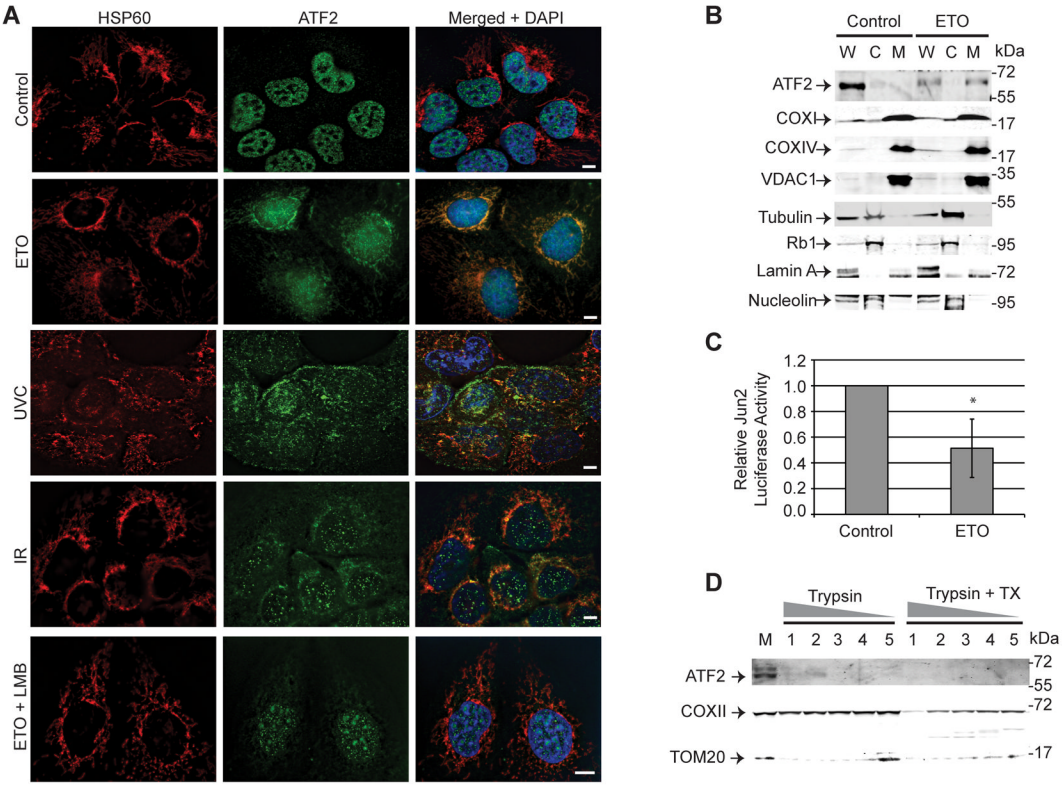

Figure 1. ATF2 localizes at the mitochondrial outer membrane in response to genotoxic stress. (See also Figure S1)

A) Control, 5 μM etoposide-treated (ETO, overnight treatment), UVC-treated (20 J/m^2), ionizing radiation-treated (IR, 5Gy), or 40 ng/ml leptomycin B (LMB) and ETO co-treated SCC9 cells grown on coverslips were immunofluorescently stained for HSP60 (red), ATF2 (green) or DNA (blue). Control and ETO panels represent 89±4% and 64±11%, respectively, of the cells from three independent replicate coverslips per condition (n > 100 cells counted per replicate). B) Control- or ETO-treated SCC9 cells were harvested for whole cell lysate (W) or biochemically fractionated to cytoplasmic (C) and mitochondrial (M) fractions, and subject to immunoblot analysis with indicated antibodies. C) Jun2 promoter-luciferase-transfected SCC9 cells were assayed for luciferase activity prior to (Control) or after ETO treatment. *: $p < 0.0001$. D) Mitochondria (M) purified from ETO-treated SCC9 cells were subject to proteolysis protection assay with titrated concentrations of trypsin: 0.2 (1), 0.1 (2), 0.05 (3), 0.025 (4), or 0.0125 (5) μg in the absence or presence of 1% Triton X-100 (TX) detergent. Scale bars represent 10 μm.

NIH-PA Author Manuscript

NIH-PA Author Manuscript

NIH-PA Author Manuscript

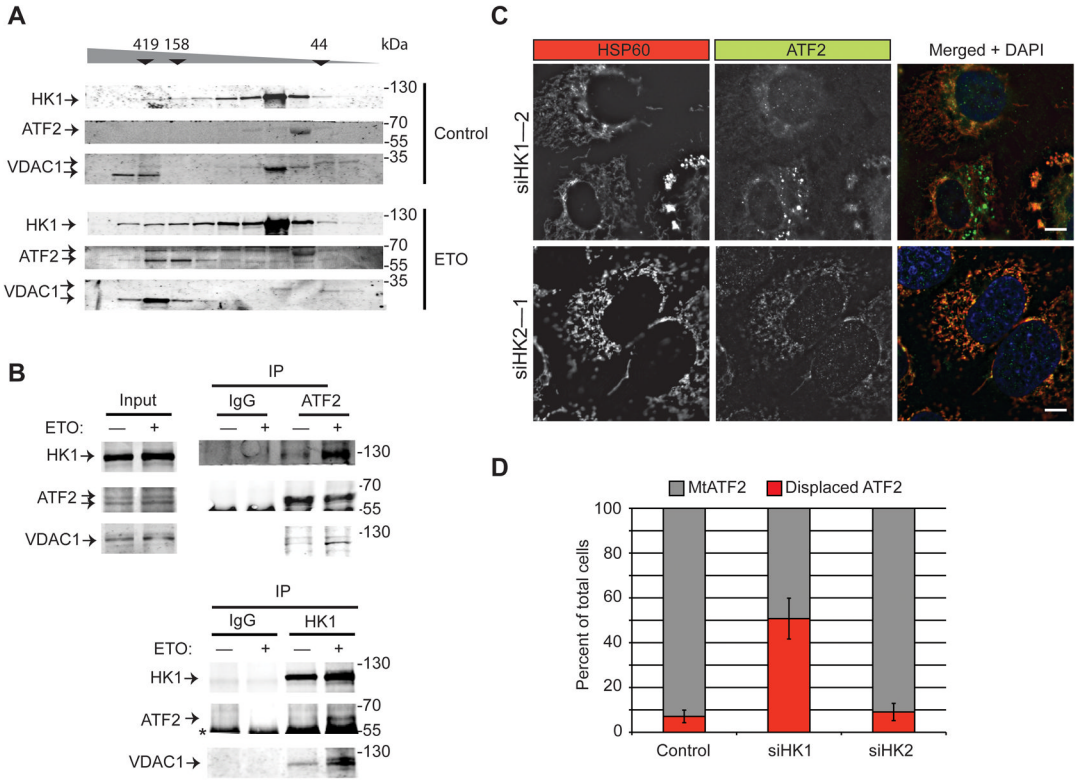

Figure 2. ATF2 interacts with VDAC1 and HK1 complex at the mitochondria. (See also Figure S2)

A) Control or 5 μM etoposide (ETO, overnight)-treated SCC9 cells were lysed and subject to size exclusion chromatography separation. Every other fraction was subject to immunoblot analysis with indicated antibodies. Fractions are arranged, left to right, in order of descending molecular weight, with control protein weight markers indicated above (in kDa). B) Control- or ETO-treated SCC9 cells were crosslinked and lysed. ATF2 (upper) or HK1 (lower) were immunoprecipitated and subject to immunoblot analysis with indicated antibodies. C) Coverslip-grown SCC9 cells knocked-down for either HK1 or HK2 and subject to ETO treatment were immunofluorescently stained with indicated antibodies. D) Quantitation of mitochondrial ATF2 (MtATF2, grey bars) versus displaced ATF2 (red bars) before or after knockdown of HK1 or HK2, n > 50 cells per replicate experiment over three independent experiments. Scale bars= 10 μm.

NIH-PA Author Manuscript

NIH-PA Author Manuscript

NIH-PA Author Manuscript

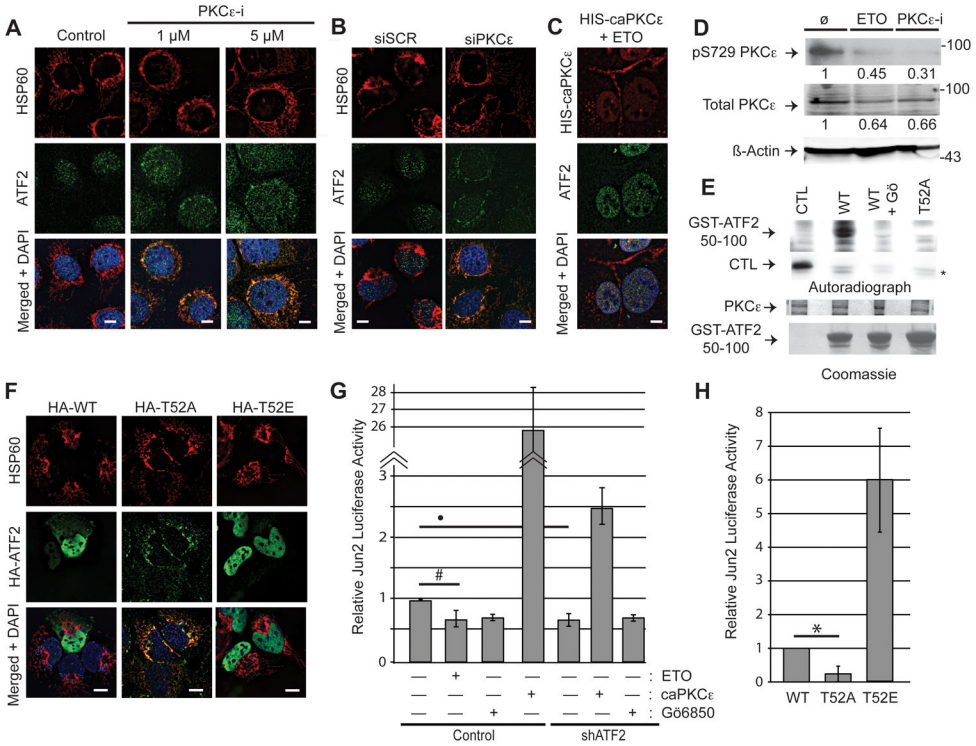

Figure 3. PKCε phosphorylation of ATF2 on Thr52 negatively regulates its mitochondrial localization. (See also Figure S3)

Coverslip-grown SCC9 cells were immunofluorescently stained with indicated antibodies after: A) overnight treatment with 1 or 5 μM PKCε translocation inhibitor (PKCε-i); B) overnight treatment with 20 nM scrambled control (siSC) or PKCε-targeted (siPKCε) siRNA; C) transfection with HIS-tagged constitutively active PKCε (caPKCε, red) and treatment with 5 μM etoposide (ETO, overnight). D) SCC9 cells treated overnight with ETO or 5 μM PKCε translocation inhibitor (PKCε-i) were lysed and subject to immunoblot analysis with indicated antibodies. E) In vitro PKCε kinase assay with Millipore control peptide (CTL), purified GST-ATF2 50–100aa WT (WT), GST-ATF2 50–100aa WT + PKCε catalytic inhibitor, Gö6850 (WT+Gö) (3) or GST-ATF2 50–100aa T52A (52A) as substrate. *: non-specific bands. Coomassie-stained gel (left) and autoradiograph (right) are displayed as indicated. F) Coverslip-grown SCC9 cells were transfected with HA-tagged wild-type ATF2 (WT), $ATF2^{T52A}$ or $ATF2^{T52E}$, and subsequently immunofluorescently stained with indicated antibodies. G) SCC9 control or ATF2 knocked-down cells (shATF2) were transfected with Jun2 promoter-luciferase construct and either empty vector (EV) or caPKCε were assayed for luciferase activity before and after overnight ETO or Gö6850 (2 μM) treatment.•: p = 0.0034; #: p = 0.0157. H) SCC9 cells stably knocked-down for ATF2 with a 3′-UTR-targeted shRNA were reconstituted with Jun2 promoter-luciferase construct and $ATF2^{WT}$, $ATF2^{T52A}$ or $ATF2^{T52E}$ and were subsequently assayed for luciferase activity. *: p = 0.0047. Scale bars represent 10 μm.

NIH-PA Author Manuscript

NIH-PA Author Manuscript

NIH-PA Author Manuscript

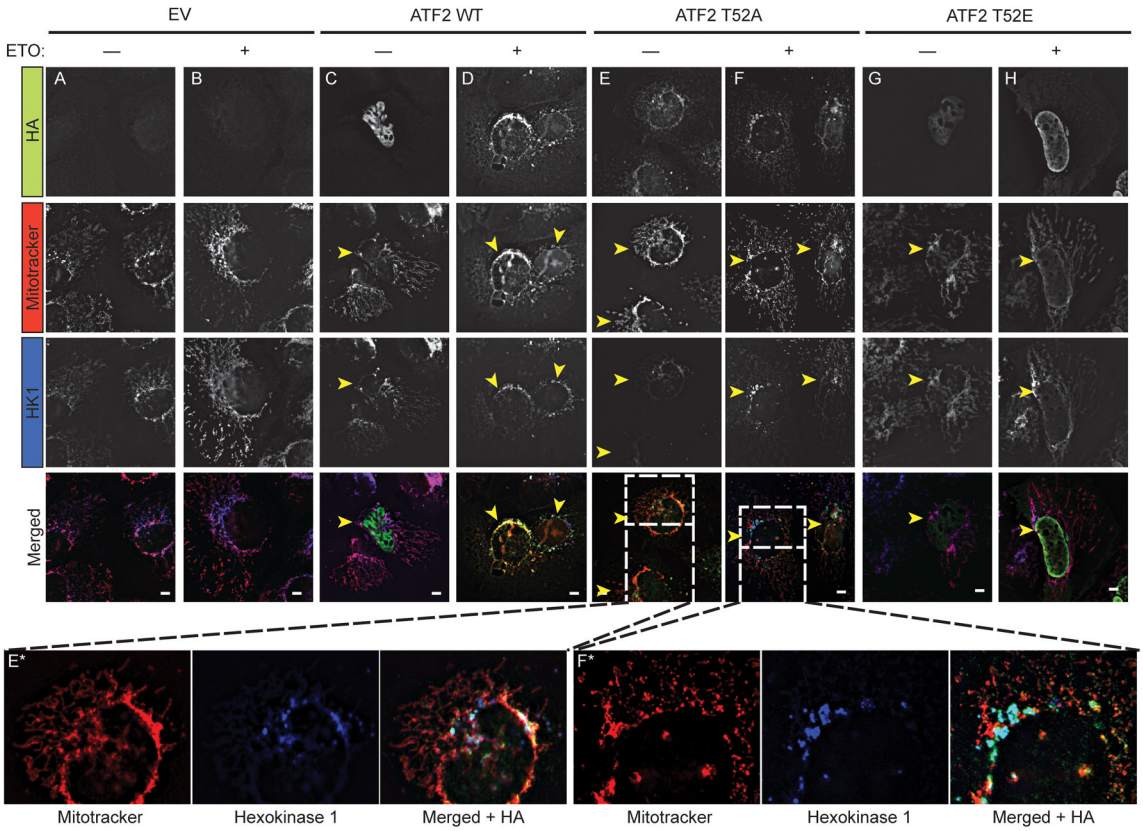

Figure 4. ATF2^{T52A} displaces HK1 from mitochondria. (See also Figure S4)

Coverslip-grown SCC9 cells were transfected with empty vector (EV) or HA-tagged ATF2 (WT), ATF2^{T52A} or ATF2^{T52E} in the absence (A, C, E, E*, G) or presence (B, D, F, F*, H) of 5 μM etoposide (ETO, overnight), and subsequently immunostained with indicated antibodies and MitoTracker. Yellow arrowheads indicate HA-positive cells. Scale bars represent 10 μm.

NIH-PA Author Manuscript

NIH-PA Author Manuscript

NIH-PA Author Manuscript

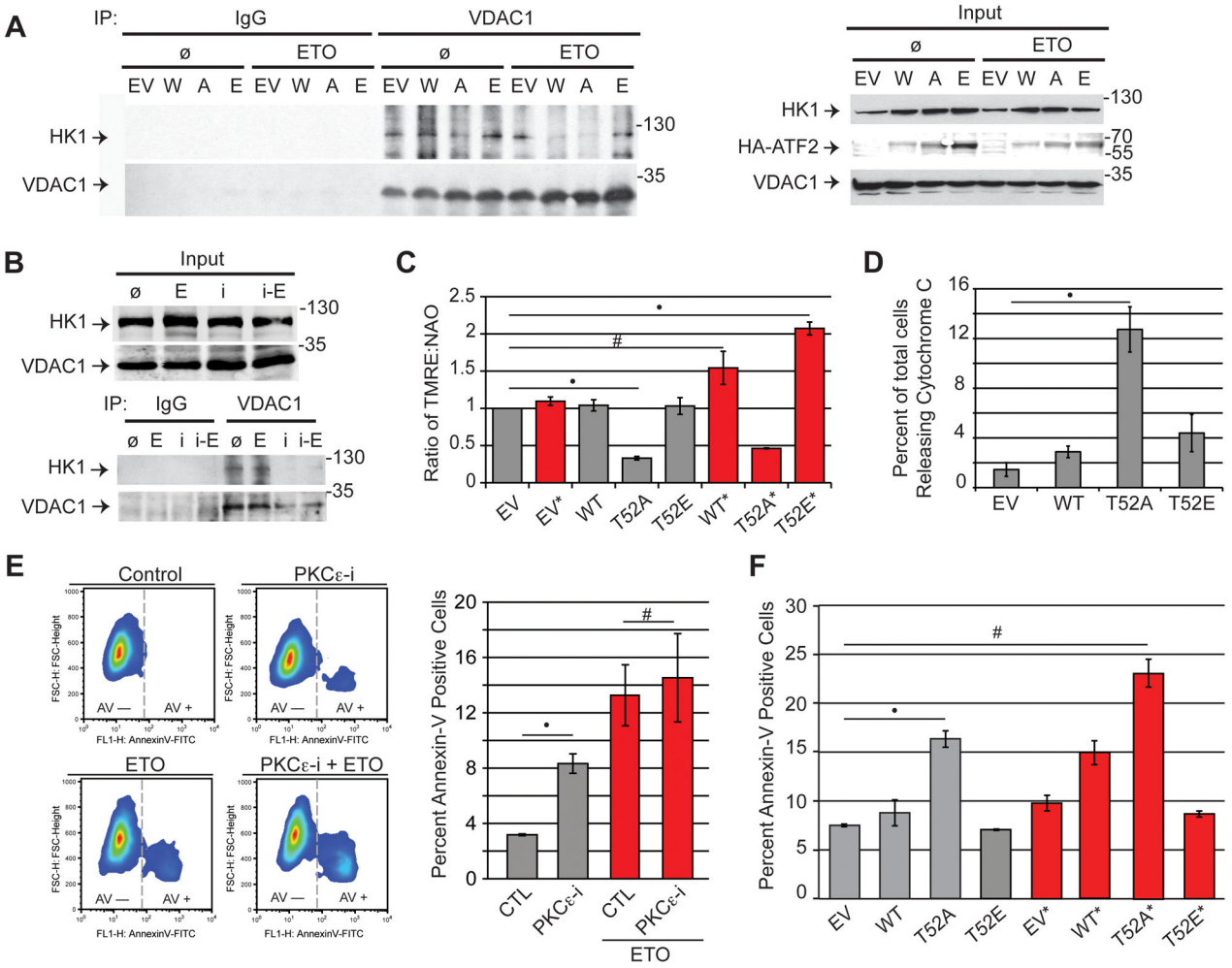

Figure 5. ATF2^{T52A} abrogates HK1:VDAC association, promoting mitochondrial leakage, cytochrome C release and cell death. (See also Figure S5)

A) SCC9 cells were transfected with empty vector (EV) or HA-tagged ATF2 (W), ATF2^{T52A} (A) or ATF2^{T52E} (E) in the presence or absence of 5 μM etoposide (ETO, overnight), crosslinked and lysed for whole cell lysate (input) or immunoprecipitated for VDAC1 and subject to immunoblot analysis with indicated antibodies. B) SCC9 cells were treated with ETO (E) or PKCε translocation inhibitor (i, 5 μM) or both (i-E), lysed for whole cell lysate (input) or immunoprecipitated for VDAC1 and subject to immunoblot analysis with indicated antibodies. C) SCC9 cells transfected with EV, W, A or E in the presence (*, red bars) or absence (grey bars) of 5 μM etoposide overnight were pulse labeled with tetramethylrhodamine ethyl ester (TMRE) or nonylacridine orange (NaO), and subsequently analyzed by FACS analysis. Histogram bars represent ratios of TMRE/NaO uptake. See Figure S4 for individual TMRE and NaO values. N = 10,000 cells per replicate; 3 replicates per condition were performed. •: $p < 0.0001$; #: $p = 0.01$ D) Coverslip-grown SCC9 cells transfected with EV, W, A or E were immunostained for cytochrome C and MitoTracker, and analyzed for cytochrome C release by fluorescence microscopy (n>100 cells per replicate; 3 replicates per condition were performed).•: $p = 0.0008$ E) Right, SCC9 cells treated with PKCε-i (5μM) alone or in the presence of ETO (overnight) were stained with Annexin-V and propidium iodide (PI) and subject to FACS analysis. •: $p < 0.0001$; #: $p = 0.6018$. Representative FACS plots (left) and corresponding Annexin V-negative and

NIH-PA Author Manuscript

NIH-PA Author Manuscript

NIH-PA Author Manuscript

Annexin V-positive (AV−, AV+) percentages are as follows: control (97%, 3%); PKCε-i (92%, 8%); ETO (89.5%, 11.5%); and ETO+PKCε-i (87%, 13%). Averaged value histograms (right) are displayed as indicated. F) SCC9 cells were transfected with EV, W, A or E in the presence (*, red bars) or absence (grey bars) of ETO. Cells were stained with Annexin-V and subject to FACS analysis. n = 10,000 cells per replicate; three replicates per condition were performed. •: $p = 0.0001$; #: $p<0.0001$

NIH-PA Author Manuscript

NIH-PA Author Manuscript

NIH-PA Author Manuscript

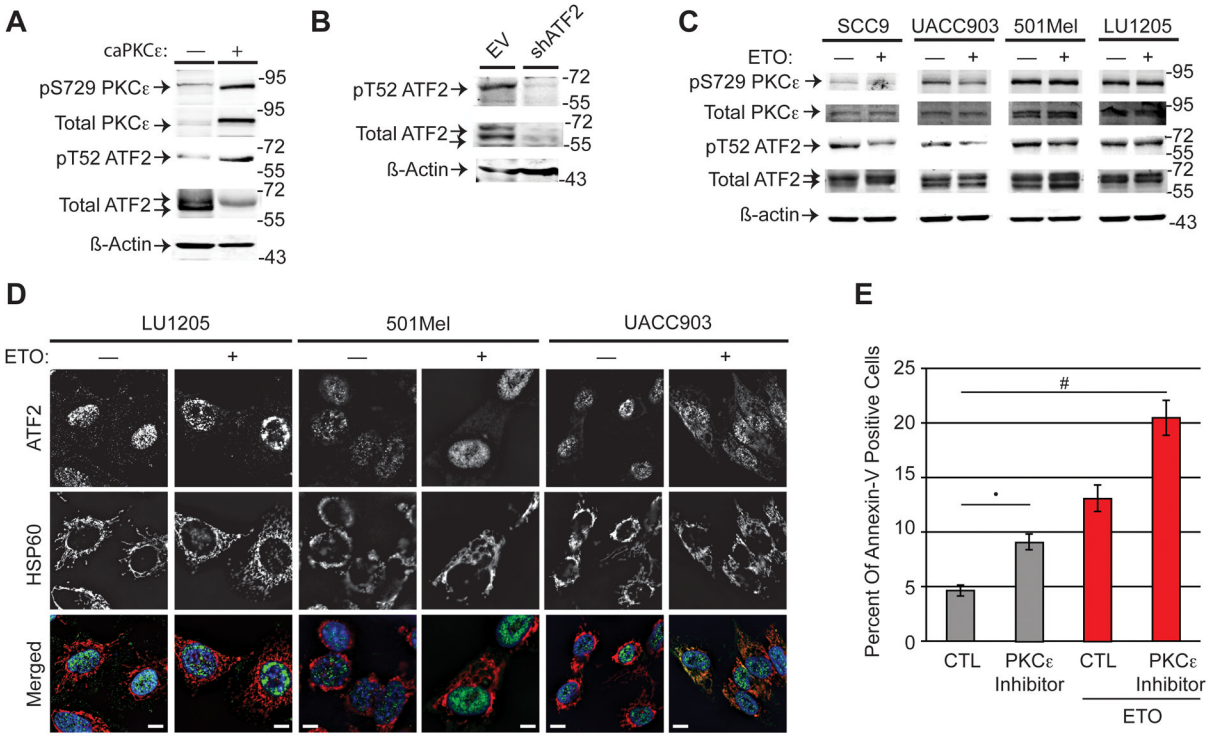

Figure 6. PKCε phosphorylation of ATF2 on Thr52 and resistance of melanoma cells to genotoxic stress-induced cell death. (See also Figure S6)

A) SCC9 cells were transfected with empty vector or constitutively active PKCε (caPKCε), and subject to immunoblot analysis with indicated antibodies. Densitometric ratios of bands for (−caPKCε, +caPKCε) are as follows: pS729/β-actin (0.193, 0.636); pT52/Total ATF2 (0.215, 0.662). B) Control or ATF2-knocked down LU1205 cells were subject to immunoblot analysis with indicated antibodies. C) Indicated cell lines were subject to (10 μM, ETO, overnight) etoposide treatment and subject to immunoblot analysis with indicated antibodies. Densitometric band ratios for pT52/Total ATF2 (−ETO, +ETO) are as follows: SCC9 (1, 0.4), UACC903 (1, 0.7), 501Mel (1, 0.9), LU1205 (1, 1). Densitometric band ratios for pS729/Total PKCε (−ETO, +ETO) are as follows: SCC9 (1, 0.7), UACC903 (1, 0.7), 501Mel (1, 0.97), LU1205 (1, 1). D) Control or ETO-treated coverslip-grown LU1205, 501Mel or UACC903 cells were immunofluorescently stained with indicated antibodies. E) 501Mel cells treated with 10 μM PKCε translocation inhibitor (PKCε-i) alone or in the presence or absence of 5 μM etoposide (ETO, overnight) were stained with Annexin-V and subject to FACS analysis. n = 10,000 cells per replicate; three replicates per condition were performed. •: $p = 0.0009$; #: $p = 0.0032$

NIH-PA Author Manuscript

NIH-PA Author Manuscript

NIH-PA Author Manuscript

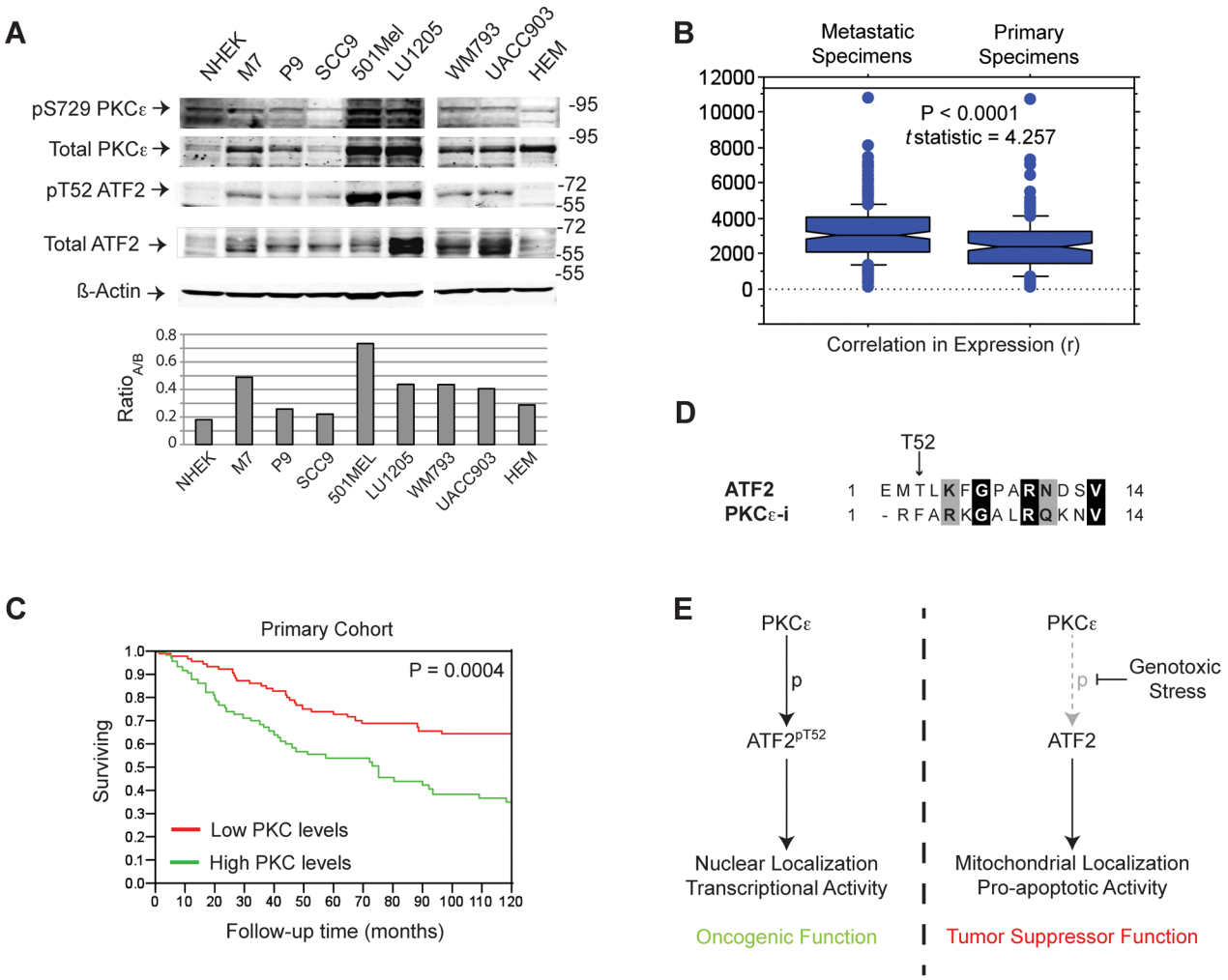

Figure 7. PKCε and phospho-T52 ATF2 expression in normal cells and malignant tumors. (See also Figure S7)

A) Primary keratinocytes (NHEK) and melanocytes (HEM), squamous carcinoma (M7, P9, SCC9) and melanoma (501Mel, LU1205, WM793 and UACC903) cell lines were subject to immunoblot analysis with indicated antibodies. Histogram represents ratio A/B, where A = densitometric ratio values of pT52/total ATF2 bands, and B = densitometric ratio values of pS729/total PKCε bands. B) Box plots showing distribution of PKCε in metastatic (left) and primary (right) specimens. PKCε levels are denoted on the Y-axis ($P < 0.0001$, t-statistic – 4.257). The mean +/− one standard deviation is depicted by the horizontal bars and is higher in the metastatic specimens. C) Kaplan Meier survival curves showing significantly shorter survival in higher PKCε expressers in primary tumors. D) Alignment of amino acid sequences flanking Thr52 in ATF2, as compared to consensus sequence used as PKCε inhibitor peptide. E) Schematic representation of PKCε-mediated regulation of the subcellular localization, and therefore, the oncogene or tumor suppressor activities of ATF2.